



Simulation of acid weathering on natural and artificial building stones according to the current atmospheric SO₂/NO_x rate

S. Gibeaux¹ · C. Thomachot-Schneider¹ · S. Eyssautier-Chuine¹ · B. Marin¹ · P. Vazquez¹

Received: 9 October 2017 / Accepted: 31 March 2018 / Published online: 3 May 2018
© Springer-Verlag GmbH Germany, part of Springer Nature 2018

Abstract

The building stones are affected by pollution. Since 1980s, the actions to reduce the greenhouse gas emissions led to the inversion of the SO₂/NO_x proportions in the atmosphere. This study aims at estimating the effects of nitrogen and sulfur compounds on stones by assessing the changes of three building limestones and one reconstituted stone submitted to acid attacks. Two of these stones were already contaminated with sulfates, while the two others were fresh quarried. Two different types of accelerated aging tests were used: (1) the exposition to two mixed acid and saturated atmospheres (HNO₃ and H₂SO₃) to simulate the ancient and current pollutants ratio and (2) the immersion in a mixed acid solution (HNO₃ and H₂SO₄) and in rainwater (pH 5 and 5.9), with and without agitation to simulate stagnant water and storm runoff water. Macroscopic, binocular and SEM observations, variations of color, weight, porosity, salt content and dissolved calcium were assessed over time. The sulfur amount influences the esthetic alterations such as color changes due to the salt precipitation and the oxidation of metallic compounds. During the immersion tests, the dissolution in the acid solution was more efficient than in the rainwater, due to the combination of the acidity and the karst effects. In the mixed acid atmospheres, the behavior of the porous network depends on the pore size distribution while in the immersion tests it is the open porosity. The high initial sulfur content of the contaminated stones increases the dissolution rate and limits the crystallization.

Keywords SO₂/NO_x · Acid rain · Acid deposition · Aging laboratory tests · Building limestone · Reconstituted stone

Introduction

Historically, the architecture of the religious edifices, castles and other magnificent buildings is the expression of the high-ranking dignitary power, explaining the willingness of their designers to use materials of excellence such as stone. However, over time and over environmental changes, the stone is altered, losing its original appearance and even its structural stability.

From the first published studies on cultural heritage conservation, the stone decay appeared clearly as depending on the type of stone and on the type of environment (Ansted 1860; Kuhlman 1863). More precisely, the alteration processes depend on the material characteristics like chemical composition, porosity and texture (Grossi et al. 1995; Massey 1999; Vazquez and Alonso 2015). Thereby, carbonate stones such as limestones, marbles and some sandstones are highly reactive to acid environments caused by pollution (Reddy 1988; Ross et al. 1989).

The urban environment is particularly aggressive for the building limestones compared to rural environment due to anthropogenic activities such as transports, industrial emissions and heating. That leads to higher concentrations of SO₂ and NO_x compared to rural environment and entails esthetical decay as yellowing, soiling or black crusts (Grossi et al. 2007; Török et al. 2011) and physical degradation as material loss and cracks (Dolske 1995; Graue et al. 2013). Those alterations are the results of the interaction between the stone components and two decay agents: atmospheric pollutants and acid rain.

This article is part of a Topical Collection in Environmental Earth Sciences on “Stone in the Architectural Heritage: from quarry to monuments—environment, exploitation, properties and durability”, guest edited by Siegfried Siegesmund, Luís Sousa, and Rubén Alfonso López-Doncel.

✉ S. Gibeaux
soizic.gibeaux@univ-reims.fr

¹ Groupe d'Etudes sur les Géomatériaux et les Environnements Naturels, Anthropiques et Archéologiques (GEGENAA, EA 3795, Université de Reims Champagne-Ardenne, 2, Esplanade Roland Garros, 51100 Reims, France

In the sheltered zones, the stone is wet but protected from leaching and the dry deposition of gaseous pollutants on the surface is favored. In the presence of water, the atmospheric SO_2 is oxidized in SO_3 and formed sulfuric acid in the moisture film. The substitution reaction of carbonates by sulfates results in salt crystallization (Török and Rozgonyi 2004; Charola et al. 2007; Grossi et al. 2007; Monna et al. 2008). The produced salt, mainly gypsum, tends to remain on the stone surface leading to crusts formation (Bai et al. 2003; Charola et al. 2007).

Nitrogen oxides (NO_x) are known mainly as catalysts for SO_2 oxidation (Massey 1999; Bai et al. 2006) than for nitrate crystallization because the oxidation of SO_2 is faster than that of NO_2 (Haneef et al. 1992). However, nitrates are soluble salts and some studies highlighted that when crystallization occurs nitrates may migrate inside the stone (Grossi et al. 1995; Camaiti et al. 2007; Vazquez et al. 2016). In urban environment, the black carbon particles (soot and fly ash) and the other pollutants emitted during fuel combustion processes agglomerate in the roughness of the gypsum crusts making particularly anesthetic decays on the stone surface such as yellowing, blackening and even black crusts (Rodríguez-Navarro and Sebastian 1996; Simao et al. 2006; Monna et al. 2008).

On the exposed zones, the wet deposition of acid rainwater affects the stone by leaching that leads to the dissolution of the carbonate components that influence the roughness, the texture and even the chemical composition of its surface (Reddy 1988; Eyssautier-Chuine et al. 2016). The rain is naturally acid, due to the solubility of the atmospheric CO_2 that makes its pH stable around 5.6. Thus, the variation of the rain acidity level depends on anthropogenic acid concentration which is mainly represented by the sulfuric and the nitric acids, products of SO_2 and NO_x oxidation, respectively (Lipfert 1989; Bonazza et al. 2009; Reddy 1988). Moreover, when precipitations come in contact with the stone, the runoff catalyzes the reaction between acids and calcite chemically considering the principle of the Collision Theory (Huber and Reid 1926; Shah et al. 2012) and mechanically by causing particles detachment (Camuffo 1995; Eyssautier-Chuine et al. 2016).

Since 1980s, the composition of the urban atmosphere has changed in Europe, particularly because the industrial manufacturers created filters to limit some pollutant emissions to respect the new limitations. Therefore, the industrial SO_2 emissions decreased highly while the nitrogen compounds coming from the traffic emissions increased. The emission ratio between SO_2 and NO_x reversed from $\text{SO}_2/\text{NO}_x = 4/1$ before 1980 to $\text{SO}_2/\text{NO}_x = 1/3$ nowadays (Massey 1999; CITEPA 2015).

Some laboratory studies, Haneef et al. (1992, 1993) and Vazquez et al. (2016), have investigated the effects of mixed acid atmosphere on carbonate stones by the use of

accelerated aging test. The chemical reactions during pollutant exposure produce color changes of the stone surface. However, the intensity of the color variation depends mainly on the initial stone color (Vazquez et al. 2016). Both studies also revealed that alterations appear faster with mixed acids than with a single component and that nitrates were systematically detected in depth within stone during a pure NO_2 and mixed $\text{HNO}_3/\text{H}_2\text{SO}_3$ atmosphere exposures.

Eyssautier-Chuine et al. (2016) simulated the effects of rain with pure solutions of sulfuric and nitric acids, in agitated and stationary conditions on limestones. The produced dissolution entailed a weight loss and the increase in the Ca^{2+} concentration in the runoff water such as noticed in previous studies (Tecer 1999; Franzoni and Sassoni 2011). The changes of intrinsic stone properties such as color, chemical composition and porosity give more relevant information for the decay degree assessment. Indeed, Eyssautier-Chuine et al. (2016) reported that color changes is related to iron oxidation of stone content and is more evident in nitric solution than in sulfuric solution and that the dissolution rate and gypsum precipitation depend on the initial total porosity, pore size distribution and pores connectivity.

The main aim of this study was to analyze and compare the reactivity of four building stones submitted to mixed acid by exposure to atmospheres and by immersion in an acid solution and in rainwater. The research strategy was to provide textural (visual observations, SEM, colorimetry), petrographic (Hg porosimetry) and chemical (EDS, ion chromatography, ICP-AES) analysis to assess qualitative and quantitative changes. The weathering kinetics were estimated by the weight changes, the measurement of sulfates and nitrates contents throughout the mixed acid exposure tests, and dissolved calcium during the immersion tests. The selected stones were three natural limestones and one artificial stone. Two natural stones were fresh quarried while the remaining limestone and the artificial stone were recovered from discarded blocks during a church restoration.

Material

This study investigated the behavior of four building stones used in the north of France and in Belgium. Two of them, the Courville limestone (Cv) and the Bajocian limestone (Bj), are extensively used in construction and were fresh quarried for this study. The two other studied stones, the Savonnières limestone (Sv) and the reconstituted stone (Rs), are widely used in heritage buildings and commonly used as replacement of original stones during restorations (Fronteau 2000). These two stones were defined as contaminated because the Sv samples stemmed from altered blocks removed from Reims monuments during restoration, and the

Rs is man-made and initially S-rich due to its fabrication (Thomachot-Schneider et al. 2011).

Fresh stones

Courville limestone (Cv)

The Courville limestone (Cv), exhibited a beige color (Fig. 1a) and fossil compounds such as Mollusca shells, miliolids and dasycladales (Fig. 1b), comes from the last stone quarry of the Marne department, and it is the most famous middle Lutetian building stone used for monument construction and restorations such as the Reims Cathedral (Fronteau et al. 2010). Its texture is matrix-supported, with partly recrystallized micritic matrix (microsparite) and secondary spar cement in the moldic macropores or in some intragranular fossil porosity (Fig. 1c). This limestone

shows an open porosity of around 20%. The mercury injection curve reveals a unimodal distribution of the pore size (Fig. 1d) that highlights one type of porosity mainly localized in the intergranular matrix. The Cv stone has a porous network with access radii relatively small, less than 0.1 μm focused around a single modal peak at 0.1 μm .

Bajocian limestone (Bj)

The Bajocian building stone (Bj) is an oolitic to bioclastic limestone (Fronteau 2000) from the French Ardennes and the south of Belgium and which is used in most of the constructions of this area. Its color is mainly russet due to iron oxide deposits visible in the porosity and over the stone surface (Fig. 1e, f). The stone is composed of calcitic debris as shell fragments, numerous echinoderm ossicles surrounded by a syntaxic cement, and Foraminifera. The

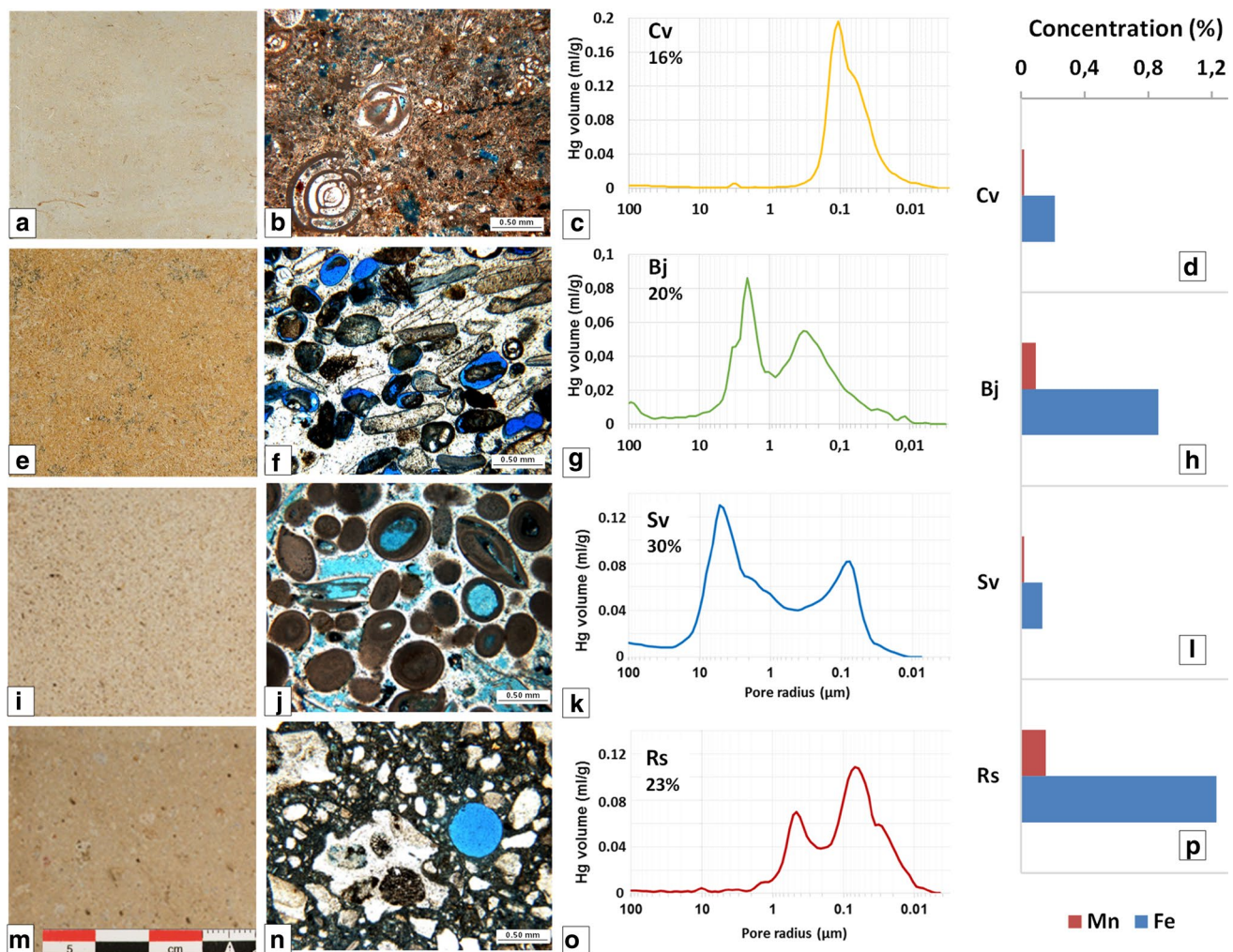


Fig. 1 Characteristics of the Courville **a–d**, the Bajocian **e–h**, the Savonnières **i–l** limestones and the Orval reconstituted stone **m–p** before the tests. Photographs (**a, e, i, m**) and blue-colored thin sec-

tions in plane polarized light (**b, f, j, n**), incremental mercury intrusion versus pore size (**c, g, k, o**) and metals content (**d, h, l, p**)

studied samples show numerous ooids surrounded by diagenetic cements, composed by calcite spar within the interstitial spaces (Fig. 1f, g). Its total porosity of around 20% shows a bimodality of the pore size distribution allocated to a low intergranular porosity and a secondary molding intragranular porosity (Fig. 1h). Bj is constituted at 90% by a ranging of pore size higher than 0.1 μm with two peaks at 2 and 0.3 μm .

Contaminated stones

Savonnières limestone (Sv)

The Savonnières (Sv) is a beige oolitic vacuolar limestone (Fig. 1i, j) extracted from the eastern part of France, for the construction of buildings from the XIX to XX centuries and is well-known to be used in current restorations in Europe (Dewanckele et al. 2014; Laycock et al. 2008). The ooliths in majority and some bivalve shells are surrounded by a sparitic cement filling partially the large and open intergranular porosity (Fig. 1j, k; Fronteau 2000; Eyssautier-Chuine et al. 2016). Its porous network is located inside the oolith nuclei and in-between the cement, and the micropores are in the oolith cortex making a bimodal pore size distribution and conferring to the stone a high open porosity with values around 30% (Fig. 1l; Dewanckele 2013; Fronteau 2000). Sv exhibits more than 50% of pore access radii superior to 0.1 μm comprising two peaks at 5 and 0.1 μm , and 30% of the intermediate range (1–0.1 μm).

Reconstituted stone (Rs)

The reconstituted stone (Rs), crafted during the last restoration of Orval Abbey between 1932 and 1948 (Thomachot-Schneider et al. 2011, 2016), has beige tones close to Bajocian colors (Fig. 1m). This synthetic material has a varied composition of limestone debris and sand bonded by a Portland cement which contains calcic lime and iron oxides (Fig. 1n) making it initially rich in silica and sulfur. The macroporosity of the Rs stone corresponds to the

air bubbles produced by the degassing during manufacture (Fig. 1n). The porous network is bimodal, with micropores located within the calcareous lithoclasts and the intermediate size pores in the matrix (Fig. 1o) and an open porosity of 23%. Rs has the highest proportion of micropores with 94% of pore access radii lower than 1 μm distributed in two peaks at 0.3 and 0.07 μm .

Methodology

Aging tests

In this study, the stones were submitted to two different enclosure conditions: (1) to reproduce the atmospheric acid deposition, the samples were exposed to the gases produced by two mixed acid and volatile solutions, and (2) to simulate the acid rain action, the stones were immersed in an acid solution with and without agitation.

Mixed acid atmosphere exposure

The acid deposition processes were assessed through accelerated aging tests based on the standard UNE-EN 13919:2003 procedures (CEN 2002). The acid atmospheres were produced by the volatility of two solutions mixing nitric and sulfurous acids with different concentrations as detailed in Table 1.

The first solution, designated as S > N, was constituted by mixing 14.4 mL of distilled water with 50 mL of H_2SO_3 (6% w/v) and 0.6 mL of HNO_3 (69% w/w). The final S > N mixture was composed by $5.6 \cdot 10^{-1} \text{ mol L}^{-1}$ of H_2SO_3 and $1.4 \cdot 10^{-1} \text{ mol L}^{-1}$ of HNO_3 to reflect the past SO_2/NO_x ratio around 4/1.

The second solution, designated as S < N, was constituted by mixing 48 mL of distilled water with 15 mL of H_2SO_3 (6% w/v) and 2 mL of HNO_3 (69% w/w). The final S < N mixture was composed by $1.9 \cdot 10^{-1} \text{ mol L}^{-1}$ of H_2SO_3 and $5.8 \cdot 10^{-1} \text{ mol L}^{-1}$ of HNO_3 to simulate the current pollution ratio around 1/3.

Table 1 H_2SO_x and HNO_3 concentrations and characteristics of the aging tests solutions with $x=3$ for acid atmosphere test and $x=4$ for acid immersion test

Solution name	$[\text{H}_2\text{SO}_x]$ (mol L^{-1})	$[\text{HNO}_3]$ (mol L^{-1})	Ratio $\text{H}_2\text{SO}_x/$ HNO_3	pH	Agitation
S > N	$5.6 \cdot 10^{-1}$	$1.4 \cdot 10^{-1}$	4/1	–	–
S < N	$1.9 \cdot 10^{-1}$	$5.8 \cdot 10^{-1}$	1/3	–	–
SNAI	$2 \cdot 10^{-6}$	$6 \cdot 10^{-6}$	1/3	5 ± 0.1	Active
SNPI	$2 \cdot 10^{-6}$	$6 \cdot 10^{-6}$	1/3	5 ± 0.1	Passive
NRAI	–	–	–	5.92 ± 0.1	Active
NRPI	–	–	–	5.92 ± 0.1	Passive

The stock solution for nitric acid was Panreac[®] 69% w/w 1.42 kg L^{-1} , and for sulfurous acid Panreac[®] 6% w/v

A volume of 65 mL of one solution was poured into the bottom of a container of 5 L to create an acid saturated atmosphere. One container was used for each type of stone with each of the solutions. Before testing, the samples were saturated in distilled water during 48 h. The slabs were put on a plastic structure keeping them out of contact with the solution (Fig. 2) and were exposed to the acid atmospheres during 28 days.

Immersion in acid solution

The effects of acid rain were determined by means of two solutions, an artificial acid mixture and a natural rainwater. The acid solution at pH 5 was carried out by mixing 600 mL of nitric acid (10^{-5} mol L⁻¹) with 400 mL of sulfuric acid ($5 \cdot 10^{-6}$ mol L⁻¹). The rainwater, at an initially pH at 5.92, was collected in a rural area during the winter period without pulverization of fertilizer and biocides. The nomenclature and the composition of the solutions are summarized in Table 1.

For each solution, two tests were performed. The first one was an immersion of the samples in the solution (passive immersion). This test assessed the karst effect by dissolution of the selected stones due to a simple contact with an acidic solution. The second test was an immersion of the samples into the solution placed in a mechanical shaker to simulate storm rain or running off water (active immersion) (Eyssautier-Chuine et al. 2016).

For each test, three slabs of each stone type were used. The triplicates were placed in a closed container of 4 l volume. Every container was fitted with dots of silicon and plastic foam to prevent contact or collision between samples, and rubbing with the bottom of the container (Fig. 2).

The experimentations were conducted for 32 days including five cycles of immersion and following drying phases.

The first cycle went on for 24 h of immersion before drying. The following four cycles involved 4 days of continuous immersion before drying. The drift of the pH solution due to the reaction between carbonate stones and the acidic solutions implied a readjustment of pH twice a day until reaching again the initially fixed pH 5. The rainwater was renewed before each cycle. The drying phase was similar for all the cycles and carried out for 64 h in an oven at 45 °C.

Analytical methods

The type, amplitude and kinetic of the stone weathering were assessed on the samples by macroscopic and microscopic observations, weight evolutions, color and porosity changes. The chemical variations over time were evaluated by the quantification of the calcium content in solutions, and the sulfates and nitrates concentrations in stone samples.

Those analyses were performed on all the sound samples and at different time of the tests as detailed in Table 2.

Macroscopic evaluation

The images of the upper face samples were taken with a Nikon Coolpix 4500 and observed with a 60x binocular magnifier on the Olympus SZH-ILLB.

Colorimetry

Color was measured with a Konica Minolta CR-400 colorimeter using the D65 illuminant and a 8-mm target diameter.

The measurements were expressed following the CIE L* a* b* and CIE L* C*h* systems (EN ISO 105-J03: 1997). The L* parameter is lightness and registers values from 0 (black) to 100 (white). The a* and b* parameters are Cartesian chromatic parameters. They vary from -60 to 60, a* from green to red,

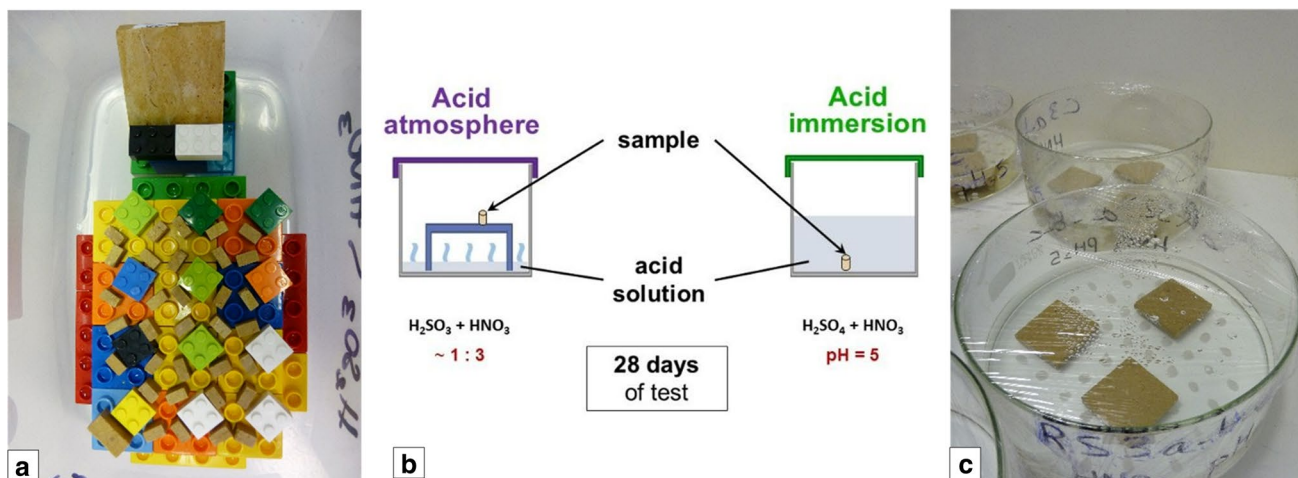
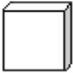
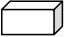



Fig. 2 Setting up of the acid immersion (a) and atmosphere (c) tests with their schematizing and characteristics (b)

Table 2 Sample dimensions depending on the performed analysis

Sample dimension	Analysis method	Analysis frequency	
		Acid atmosphere test	Immersion test
 5x5x1 cm	Macroscopic and microscopic evaluations	At the end of the experiment	
 1x1x2 cm	Colorimetry Weight Hg porosimetry	At the end of the experiment At the end of the experiment	After 4, 11, 18, 25 and 32 days
 1x1x0.4 cm	SEM–EDX	After 2, 5, 8, 14, 22 and 28 days	At the end of the experiment
Solution	Ion chromatography ICP–AES	One per day –	After 4, 11, 18, 25 and 32 days

and b^* from blue to yellow. The C^* parameter is chroma or saturation. The higher the chroma is, the more vivid the colors are. For our device, values went from 0 to 60. The h^* parameter is the hue (i.e., the tone of the stone) with values from 0 to 360° in the chromatic sphere. Thus, both depend on a^* and b^* . The ΔE^* value is introduced as the total color change to compare the variations before and after the tests as follows:

$$\Delta E^* = [(\Delta L^*)^2 + (\Delta a^*)^2 + (\Delta b^*)^2]^{1/2} \quad (1)$$

$$C^* = \sqrt{(a^{*2} + b^{*2})} \quad (2)$$

$$h^* = \arctan(b^*/a^*) \quad (3)$$

A ΔE^* value higher than 3 is considered as a visual change. The average of each parameter was calculated from 40 points measured on each slab surface, calculated previously as the minimum of measurement necessary to obtain a representative average for all the stones (Vazquez et al. 2013).

Weight changes

The weight of the stone samples was measured by an analytical balance Mettler Toledo with a sensitivity of 1 mg. The percentage of the weight variation was calculated with respect to the initial weight at the end of the acid atmosphere tests, and regularly at the end of each cycle of the immersion tests.

The surface recession has been estimated for each stone type according to the following equation based on the method used in Grossi et al. (1995):

$$R = \frac{\Delta W \times 10^4}{A \times d \times [\text{CaCO}_3]}$$

With R the recessed surface in μm , ΔW the difference between the weight at the end of the test and the initial weight in g, A the total sample surface equal to 70 cm^2 , d the calcite density equal to 2.71 g cm^{-3} (Reeder 1983) and $[\text{CaCO}_3]$ the calcite content specific to each stone based on the data of Eyssautier-Chuine et al. (2016).

Mercury intrusion porosimetry

Porosity characterization was obtained using an Hg intrusion porosimeter (MIP) Micromeritics Autopore IV 9500, reaching a 230 MPa pressure and measuring pore radii sizes from 0.002 to 180 μm . The porosity was measured on the fresh stones and on the triplicates of each stone type of size $1 \times 1 \times 2 \text{ cm}$ at the end of the atmosphere test. After the immersion test, one specimen of each altered stone type was cut in dry condition to obtain smaller sample with optimal dimensions for this measurement. The reason of not having a previous cut adapted sample is the aggressivity of the immersion test that could disintegrate completely some stone types. Parameters calculated from Hg porosity were the mean pore access radius (R_m), the modal peaks and the percentage of pores in four different pore access radius ranges: large ($> 1 \mu\text{m}$), medium ($1\text{--}0.1 \mu\text{m}$), and small ($< 0.1 \mu\text{m}$).

Scanning electron microscopy

The SEM Hitachi TM-1000 Table Top coupled to a Swifted-TM Energy-Dispersive X-Ray (EDX) was used to acquire high-quality images of precipitation crystals or dissolution details in the back-scattered electron mode and 15 kV accelerating voltage.

Sulfates and nitrates concentration (ion chromatography)

To determine the salt content in stones, the samples were powdered, brought into solution in 1 mL of ultrapure water, agitated during 12 h and centrifuged at 13,400 rpm during 10 min. The liquid phase was collected, and the process was repeated once to dissolve all the anions.

The quantity of nitrates NO_3^- and sulfates SO_4^{2-} was measured by ion chromatography with a Dionex ICS 2000 liquid chromatograph fitted out a pump, an eluent generator (EGC III) with potassium hydroxide (KOH) cartridge, an AS50 injector and a DS6 conductivity cell. The separation of anions was performed on a 2-mm Dionex IonPac AS17 column coupled to a 2-mm Dionex ASRS 300 suppressor.

Instrument control and data acquisition were performed using Chromeleon® software. The obtained curve over time, started at time $t=0$, was smoothed by using the simple exponential operation (Gardner 2006) following this sequence:

$$\begin{cases} Y_0 = C_0 \\ Y_t = \alpha C_t + (1 - \alpha)C_{t-1} \end{cases}$$

where C is the measured concentration, Y the predicted concentration and α the smoothing factor with $\alpha=0.25$.

RUNSALT simulations were carried out to predict the chemical compositions of the salts produced during the test in function of the relative humidity. RUNSALT is a graphical user interface to the ECOS thermodynamic model for the prediction of the behavior of salt mixtures under changing climate conditions (Price 2000, Bionda 2005). The amount of Ca^{2+} present in the building stones was considered in excess, and the sulfate and nitrate molar amount were chosen according to the past and current SO_2/NO_x ratio and the solution concentrations as following:

- For the $S > N$ test, $\text{SO}_4^{2-} = 3.6 \cdot 10^{-2}$ mol, $\text{NO}_3^- = 9.1 \cdot 10^{-3}$ mol, $\text{Ca}^{2+} = 4.1 \cdot 10^{-2}$ mol
- For the $S < N$ test, $\text{SO}_4^{2-} = 1.3 \cdot 10^{-2}$ mol, $\text{NO}_3^- = 3.9 \cdot 10^{-2}$ mol, $\text{Ca}^{2+} = 3.3 \cdot 10^{-2}$ mol

Dissolved Ca concentrations (ICP-AES)

The concentrations of Ca were measured in acid solutions of each cycle by inductively coupled plasma-atomic emission spectrometry (ICP-AES, Iris Advantage, Thermo Fisher Scientific). The analysis of Ca was conducted at wavelength of 184.006 through three measurements of 10 mL of each solution.

Results

Visual observations

Atmosphere tests

The both types of weathering tests led to naked-eye detectable changes, notably color differences, salt precipitations and dissolution patterns that depended both on the type of stone and test.

Concerning the acid atmosphere exposure, the macroscopic observations showed a yellowing of every stone with the two concentrations. Specific features were observed for the $S < N$ test such as a located blackening of Bj and Rs and white spots on the Cv sample (Fig. 3). After 28 days, all the stone surfaces were covered by a salt crust independently of the acid proportion. The binocular magnifier observations showed a smooth crust on Cv with the presence of white spots looking like rhombic gypsum after the $S < N$ test. For the other samples, the intuitive crystals' shape was visible especially inside ooids on Sv and Bj (Fig. 4).

Immersion tests

After the immersion tests, all the stones darkened except Cv that lightened in the SNPI and the NRAI. The yellowing was evident to the naked eye on all the stones for the SNAI test (Fig. 3).

The observations with binocular magnifier detailed the esthetic alterations due to acid immersion affecting the stone components, such as discoloration and erosion (Fig. 4). The rainwater did not produce notable changes on the stones. The stirring did not result in different weathering compared to the motionless solution, though the iron oxidation occurring on each stone as well as the dissolution patterns were more intense in active than in passive condition.

On Cv, the oxidation of the Fe-containing calcitic cements which was identified as russet tones started after the second cycle of immersion/drying in the acid solutions. At the end of the active immersion test, the color changes affected the Foraminifera (Fig. 4). The ooids of the Bj samples were the first concerned by the oxidation. Later, after the second cycle, the russet color of the components and the cement was intensified and spread through the whole surface. The cement of Sv did not seem affected until the end of the test contrary to the ooliths whose cortex was oxidized and partially dissolved producing an increase in the surface roughness. The effects of the acid contact with Rs surface were clearly and progressively visible. The lithoclasts showed preferential dissolution and the russet oxidation affected the components more than the matrix at the end of the tests.

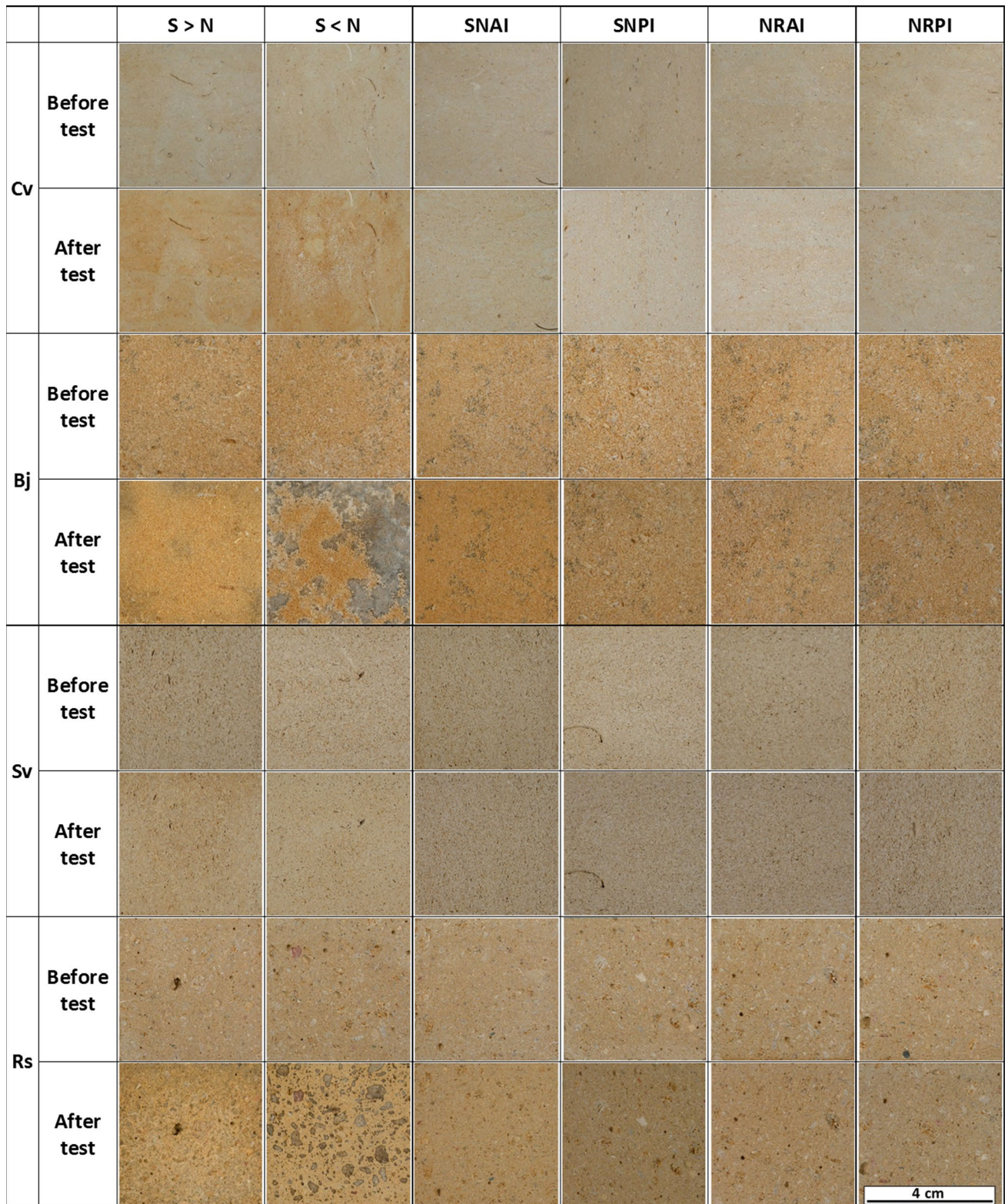


Fig. 3 Photographs of entire stone samples before and after the mixed acid exposure tests (S > N mixed acid atmosphere with a ratio S:N=4:1, S < N mixed acid atmosphere with a ratio S:N=1:3) and the immersion weathering tests (SNAI sulfuric and nitric active

immersion, SNPI sulfuric and nitric passive immersion, NRAI natural rainwater active immersion and NRPI natural rainwater passive immersion)

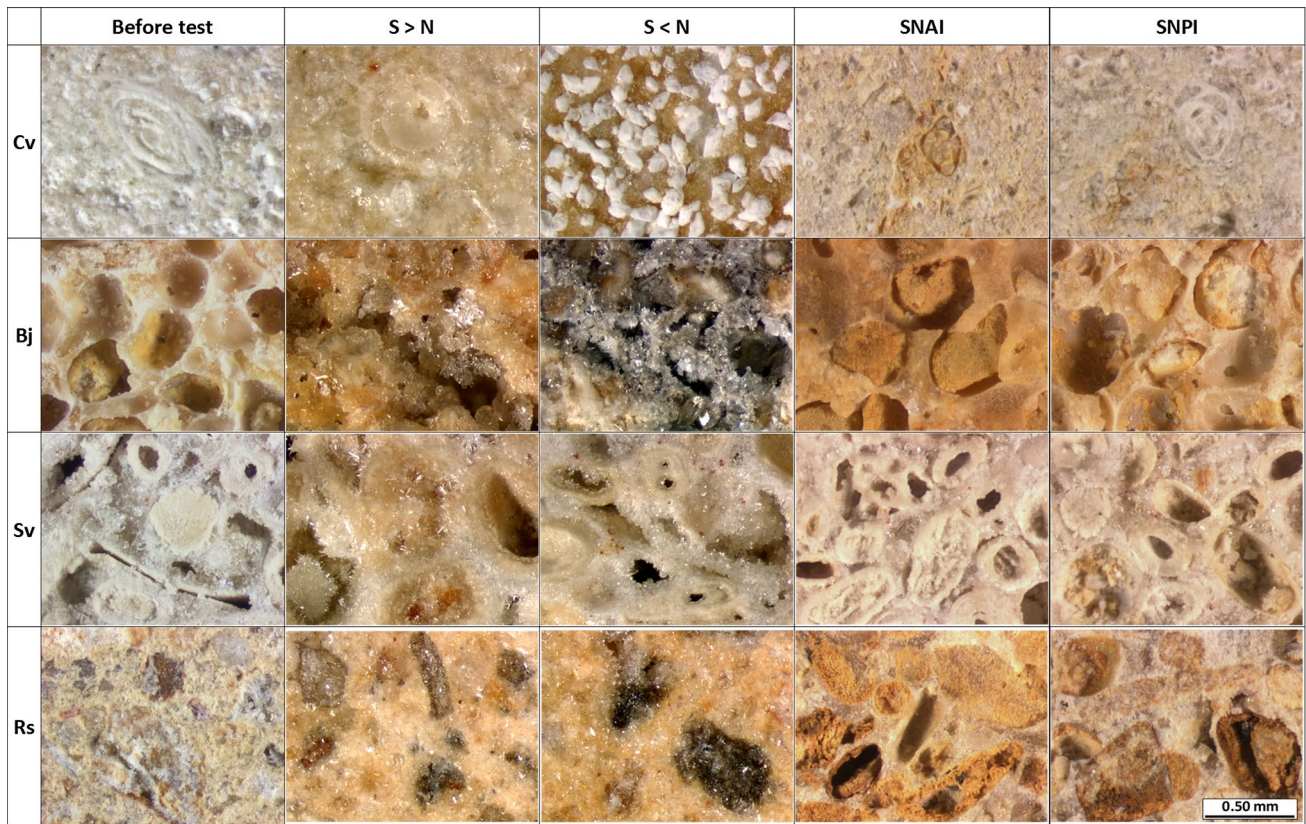


Fig. 4 Details of stones before (fresh samples) and after the acid atmosphere ($S > N$ and $S < N$) and the acid immersion (SNAI and SNPI) tests

Table 3 Ranges of the chromatic values for the fresh samples

Stone	L^*	C^*	h^*
	Min–Max	Min–Max	Min–Max
Cv	75.6–81.8	14.6–19.4	95.2–100.8
Bj	66.8–73.7	19.4–29.2	74.8–79.6
Sv	72.4–78.2	16.1–20.7	91.8–96.8
Rs	66.9–74.4	16.7–23.4	77.3–79.9

Colorimetry

The initial chromatic parameters of each stone are detailed in Table 3.

Atmosphere tests

All the acid atmosphere exposure led to naked-eye detectable color changes, confirmed by $\Delta E^* > 3$. In general, these variations resulted from a decrease in the lightness of the stone surface ($\Delta L^* < 0$), a variable evolution of the chroma and an opposite behavior of the hue, with Cv and Sv that changed evidently their tone against Bj and Rs that kept

their tone intact (Fig. 5). Regarding the type of test, in general $S > N$ led to higher or similar changes than $S < N$, with the exception of chroma parameter for Bj stone, which showed contrary trend. At the end of the exposures, Cv underwent the most important color variations with high delta values for all the parameters.

Immersion tests

In most of the cases, immersion test produced a visible total color change on the studied stones ($\Delta E^* > 3$). In this case, the trends were a slight variation in lightness and chroma, more evident in Cv and Rs, and hue that behaved similarly to acid atmosphere exposure, with great changes in Cv and Sv for all the test while Bj and Rs remained unchanged. In general, active immersion led to higher or similar changes than passive, with remarkably high values in Bj and Sv for L^* and C^* . The differences between the immersion in an acid solution and the natural rainwater were negligible, with sometimes even higher differences measured after natural rainwater test.

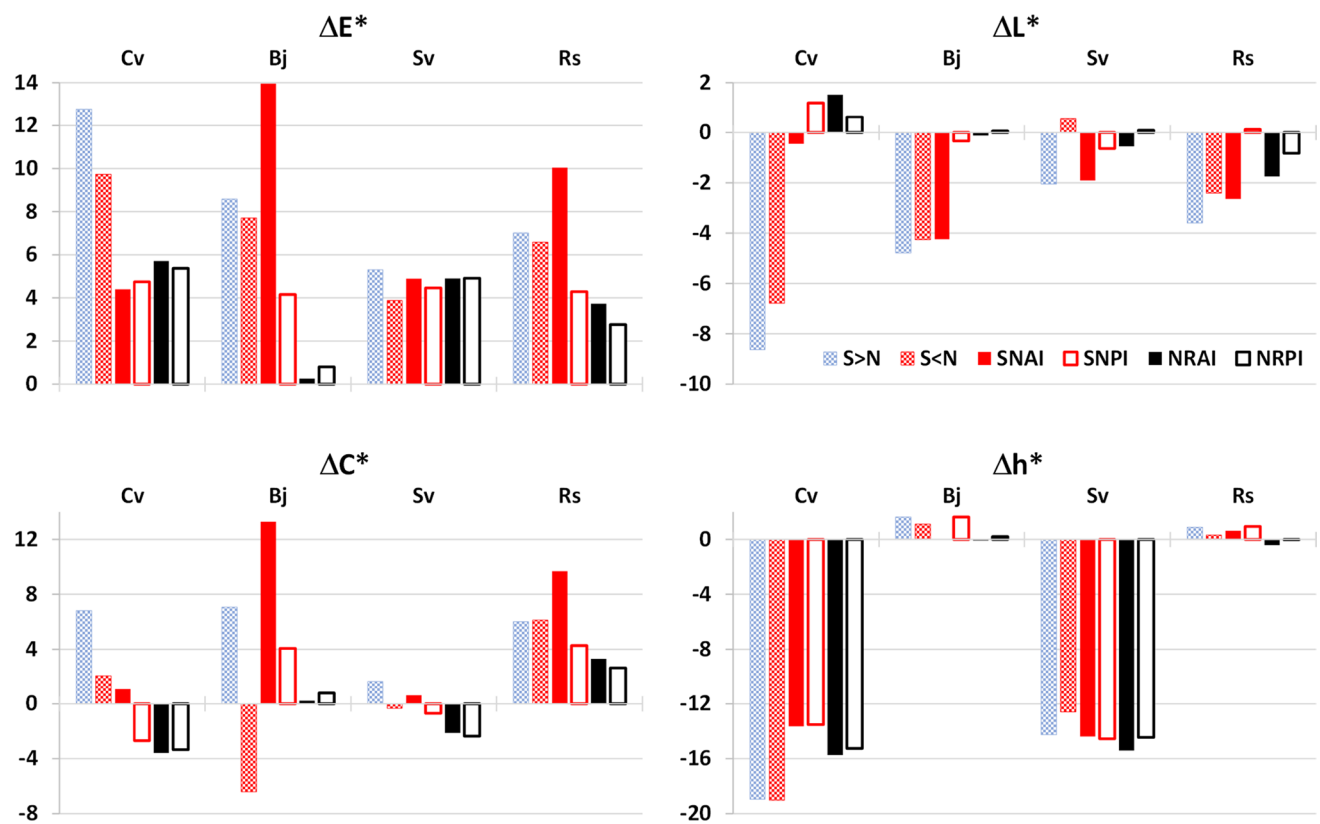


Fig. 5 Variations of chromatic parameters before and after the weathering tests

Weight changes

After the exposure to acid atmospheres, the gain of weight was evident while, the stones tended to lost matter after the immersion tests.

Atmosphere tests

The weight increased for the both tests, but the gain was higher in the $S > N$ test with between 0.6% and 1.2% (Fig. 6a). For $S > N$ concentration, Sv and Rs showed the highest weight gain ($> 1\%$) while Cv and Bj experimented less changes ($\approx 0.6\%$). For $S < N$ concentration, the weight gain was less significant, with the lowest values for Rs (0.2%).

Immersion tests

For all the samples and tests, the weight decreased over time and stabilized slightly thereafter. The samples immersed in the acid solutions exhibited higher surface recession than in natural rainwater. In the mixed acid

solution, all the stones showed a material loss more noticeable in active than in passive immersion (Fig. 6b).

After the immersion in natural rainwater, the material losses were negligible for Cv and Bj ($< 5 \mu\text{m}$) while Sv and Rs showed values up to $40 \mu\text{m}$ (Fig. 6b). Only Rs revealed differences between the results of active and passive immersion ($\Delta R = 10 \mu\text{m}$).

After the immersion in acid and active immersion, Cv and Bj had the lowest and comparable surface recession values ($\approx 30 \mu\text{m}$) while Sv and Rs had the highest loss ($\approx 75 \mu\text{m}$).

Pore access radii

The open porosity values and the evolution of the pore size distribution obtained by Hg intrusion porosimetry are exposed in Table 4 and Fig. 7.

Atmosphere tests

The open porosity did not vary after the exposure of all the stone types to the $S > N$ atmosphere (Table 4). However, for the $S < N$ test, open porosity increased notably in Bj up to 5% but less in Sv up to 1.9%, while it decreased in Cv around 1.5%. The change was insignificant for Rs.

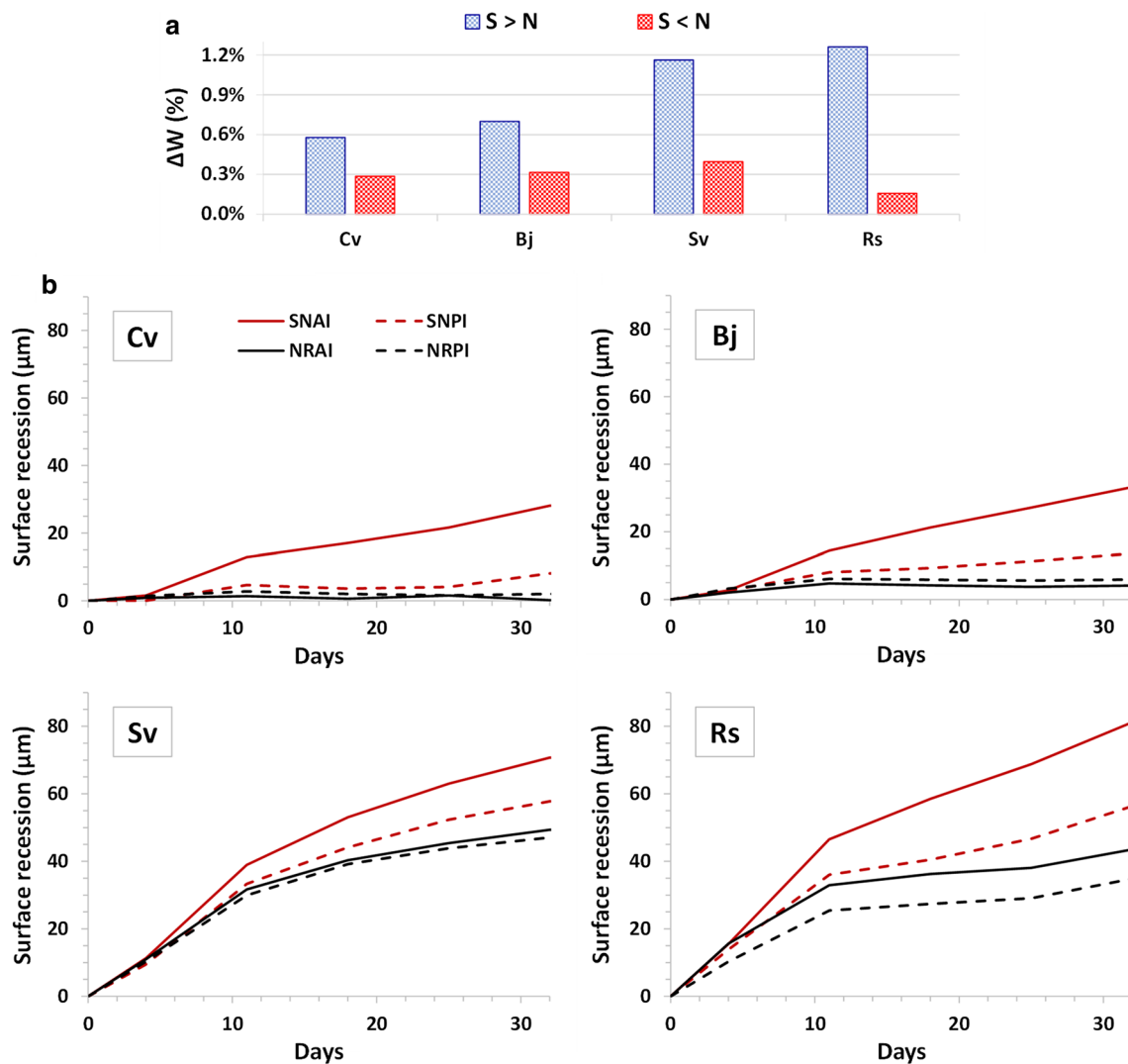


Fig. 6 Weight variations ΔW , expressed in percentage in respect to the initial weight, at the end of the atmosphere exposure tests (a) and calculated surface recession during the immersion tests (b)

The pore access radii distribution showed different evolutions depending on the stone and the test. Cv and Rs exhibited evident variations for both concentrations (Table 4, Fig. 7). For Cv, the access radii of the existent pores widened for the S > N while for the S < N the proportion of modal pores increased (Fig. 7a). For Rs, the pore access radii comprised between 0.4 and 2 μm narrowed after both tests and those between 0.2 and 0.4 μm closed (Fig. 7d).

For Bj and Sv, the differences in the pore size distribution were more evident, with similar behaviors for pore radii > 1 μm (decrease for S > N and increase for S < N) and the contrary for the other intervals. Bj showed an increase of 1–0.1 μm range and a decrease of the <0.1 μm range, with higher difference in S < N test (Fig. 7b). Sv porosity experimented an augmentation in 1–0.1 μm range for both tests (Fig. 7c).

Immersion tests

After the acid immersion tests, the variations of the open porosity were low and evolved in function of the stone and the test (Table 4). After the SNPI test, the porosity increased for all the stones while in the SNAI test, Cv and Rs porosity trended to decrease. Concerning the natural rain immersion, the agitation of the solution did not influence the variation of open porosity that increased for Sv and Rs and decreased for Cv and Bj.

Concerning the pore access radii evolution, Sv appeared less affected by the immersion tests with maximum variations in the SNPI solution resulting in a decrease in the larger pore access (> 1 μm) and an increase in the intermediate pore access (1–0.1 μm) (Table 4; Fig. 7g). Some trends were observed in relation to the solution composition, regardless of the stirring

Table 4 Porosity parameters before and after the mixed acid weathering tests (calculated from Hg porosimetry)

Stone	Test	Porosity (%)	Pore size distribution (%)		
			> 1 μm	1–0.1 μm	<0.1 μm
Cv	Fresh	20.1 \pm 3.3	4 \pm 1	22 \pm 10	74 \pm 9
	S > N	20.4	5	49	46
	S < N	18.6	6	25	69
	SNAI	20.1	5	35	60
	SNPI	20.9	3	35	62
	NRAI	19.4	3	26	71
	NRPI	18.1	3	16	81
Bj	Fresh	20.0 \pm 1.0	47 \pm 2	42 \pm 1	11 \pm 2
	S > N	20.4	45	47	8
	S < N	24.9	56	36	8
	SNAI	23.1	55	36	9
	SNPI	22.2	53	37	10
	NRAI	19.4	44	46	10
	NRPI	19.9	43	45	12
Sv	Fresh	31.8 \pm 0.6	58 \pm 3	29 \pm 3	13 \pm 4
	S > N	30.9	55	30	15
	S < N	33.7	54	33	13
	SNAI	33.5	55	30	15
	SNPI	32.8	54	31	15
	NRAI	34.7	58	27	15
	NRPI	34.5	54	31	15
Rs	Fresh	22.9 \pm 1.6	6 \pm 1	41 \pm 4	53 \pm 4
	S > N	22.6	5	36	59
	S < N	22.7	5	39	56
	SNAI	22.6	3	30	67
	SNPI	23.8	3	34	63
	NRAI	24.5	6	47	47
	NRPI	24.2	6	31	63

The initial state values are given with their standard deviation. The values in bold are outside the range of the natural variations of each stone porosity

mode. In the natural rainwater, the pore size changes were negligible except for Cv and Rs in NRPI that both showed a loss of intermediate pores and a gain of small pores (Fig. 7e, h; Table 4). For the same open porosity values, in the mixed acid solutions the amount of the largest pores increased in Bj while the smallest decreased in Cv. The intermediate behaved contrarily, with a decrease in Bj and increase in Cv (Fig. 7e, f). The smallest range of pore size increased notably in Rs, unlike the intermediate pore radii suffered a diminution (Fig. 7b; Table 4).

SEM observations

Atmosphere tests

The SEM images obtained during the acid atmosphere tests showed the formation of salt crystals from the very first day to the end of the tests that confirmed and specified the salt habitus depending on the type of stone and test (Fig. 8). No evolution over time in the crystals shape or size was detected for each sample and test. During the S > N test, Cv and Bj surfaces displayed platy crystals, while on Sv and Rs, the crust was composed by a mix of cauliflower and needle-like crystals. For the S < N exposure, Bj and Sv exhibited arrow-like crystals, Rs needle-like crystals and Cv rhombic-shaped crystals.

Immersion tests

After the acid immersions, the samples in contact with rainwater did not display any dissolution feature on the SEM images, while the samples submitted to the acid solution showed different ones depending on the stone. The dissolution patterns in the latter were similar in the active (SNAI) and passive (SNPI) tests and affected mainly the fossils in Cv and Bj, the cortex of the oolites in Sv and the calcareous components in Rs (Fig. 8). Neither sulfate nor nitrate crystals were observed on SEM, but sulfur was detected by EDX with an amount comprised between 1 and 5%.

Chemical assessment

Sulfates and nitrates concentrations in stones

During the atmosphere tests, the amount of sulfates SO_4^{2-} in the stones increased during the first days for both tests, followed by a weak trend to augmentation or even stabilization except for Sv which showed no variation with time (Fig. 9). Sv and Rs were initially S-rich with concentrations in SO_4^{2-} of 4 and 2 mg g^{-1} , respectively, versus negligible for the fresh stones.

During the S > N exposure, Rs, Cv and Bj showed similar kinetics despite the initial content the SO_4^{2-} concentration with a maximal increase of 2.5 mg g^{-1} (Fig. 9a). For the S < N test, Bj and Rs kinetics were similar to those of S > N test and Cv showed lower final values than the other stones (Fig. 9b). The SO_4^{2-} concentration remained constant for Sv through all the tests.

Nitrate formation differed to the sulfate one. A linear increase was observed only for Cv and Bj in the S > N test. The nitrate concentrations in the other stones and tests could be considered negligible in this study.

At 20 °C, Runsalt simulations indicated the possible crystallization of gypsum $\text{CaSO}_4 \cdot 2\text{H}_2\text{O}$ at any humidity, and

nitrocalcite $\text{Ca}(\text{NO}_3)_2$ below 52% RH in the case of the two tests $S > N$ and $S < N$.

Dissolved Ca concentration

The concentrations of Ca^{2+} in the solutions due to stone dissolution increased with time for all the stone types during all the used weathering methods (Fig. 10). Sv and Rs showed the highest Ca^{2+} loss whatever the test. Clear differences were likewise observed between acid and rainwater solutions, and between active and passive immersions. The final Ca^{2+} concentrations were maximal in the mixed acid and agitated solution reaching around 600 mg L^{-1} for Sv and Rs, and 400 mg L^{-1} for Cv and Bj. The passive results were also grouped by contaminated and fresh stones, with 500 mg L^{-1} for Sv and Rs, and 150 mg L^{-1} for Cv and Bj. In natural rainwater, Cv and Bj were hardly dissolved even in the agitated system. Sv behaved similarly than in the mixed acid solution, and Rs showed intermediate dissolution compared to the rest of the stones.

Discussion

The contact of limestones with rain and acidic polluted atmosphere led to chemical reactions between the stone components, specially calcite, and the sulfurous and nitric acids. The immersion of the samples in an acid solution and the exposure to an acid environment revealed esthetic and structural alterations depending on external factors such as the type and conditions of test, and on inherent stone characteristics such as composition and porosity.

Weathering tests

Differences between acid tests (atmosphere-immersion)

The main difference between acid tests was measured as weight changes, with a gain for acid atmosphere exposure due to gypsum precipitation, and a loss in acid immersion due to dissolution.

The precipitation of salts in the acid atmosphere exposure occurred from the first day and remained stable until the end of the test as shown by SEM observations while during the immersion test, the salt precipitation occurred only during the four drying stages (Eyssautier-Chuine et al. 2016). That explains that only in the atmosphere exposition test the precipitated salt was visible and up to 10 times higher than in the immersion test after being measured by ion chromatography.

The gypsum is the product of two successive reactions: (1) the dissolution of calcite by acids, called acidity effect

(Lipfert 1989) and (2) the substitution of carbonate by sulfates as follows:

1. $\text{CaCO}_{3(s)} + \text{H}_2\text{SO}_4 = \text{Ca}^{2+} + \text{SO}_4^{2-} + \text{H}_2\text{O} + \text{CO}_2$
2. $\text{Ca}^{2+} + \text{SO}_4^{2-} = \text{CaSO}_{4(s)}$

In the case of the clean rainwater, the dissolution of calcite is due to the inherent acidity of the solution due to atmospheric carbon dioxide presence, called karst effect (Lipfert 1989; Webb et al. 1992).

The material loss affecting the immersed stones was confirmed by the decrease in weight and the calcium loss. The dissolution stage preceding the crystallization process during the acid atmosphere tests was highlighted by the Hg porosimetry results showing the widening of the pore access radii (Tecer 1999; Vazquez et al. 2016).

Influence of the fluid chemical composition

To develop the atmospheric tests, the ratios $\text{H}_2\text{SO}_3/\text{HNO}_3$ were chosen to represent the past and the current environmental pollution ratio, respectively, $S > N$ (4/1) and $S < N$ (1/3). From any point of view, $S > N$ appeared more aggressive than $S < N$.

Macroscopically and regarding the SEM observations, even if salt crystals' shape were different for each stone, the $S > N$ test showed a better coverage of the surfaces. These results were also corroborated by a decrease in the lightness, a higher weight gain and ion chromatography results. The preexistent gypsum content in Sv limited its reactivity to the acid atmosphere. The presence of sodium sulfate in Rs did not prevent the precipitation of calcium sulfate. The nitrogen-based salts appeared only in non-contaminated stones (Cv and Bj) for the $S > N$ test that indicated the relationship between nitrate precipitation and the sulfur content.

The total recession and the natural recession increased at higher porosities which is especially evident for the natural solution, in the case of very high porosity stones such as the Savonnières limestone Sv (Table 5; Franzoni and Sassoni 2011). Regarding its low acidity and its origin, the rainwater used during the immersion tests could be considered as "clean rain" and as the karst effect factor in the surface recession models (Lipfert 1989; Livingston 1992; Webb et al. 1992). As suggested by Cardell-Fernández et al. (2002) and Bonazza et al. (2009) and confirmed by the results of this study, the Lipfert model overestimated the karst effect which appeared as the dominant contributor in the dissolution of carbonate stones surface by the action of the rainwater runoff on buildings. While the Livingston and Webb models underestimated the nitrate fraction implied in the dissolution (Cardell-Fernández et al. 2002). Those models could arise limited in terms on simulating the current and future atmospheric pollution. However Franzoni and Sassoni

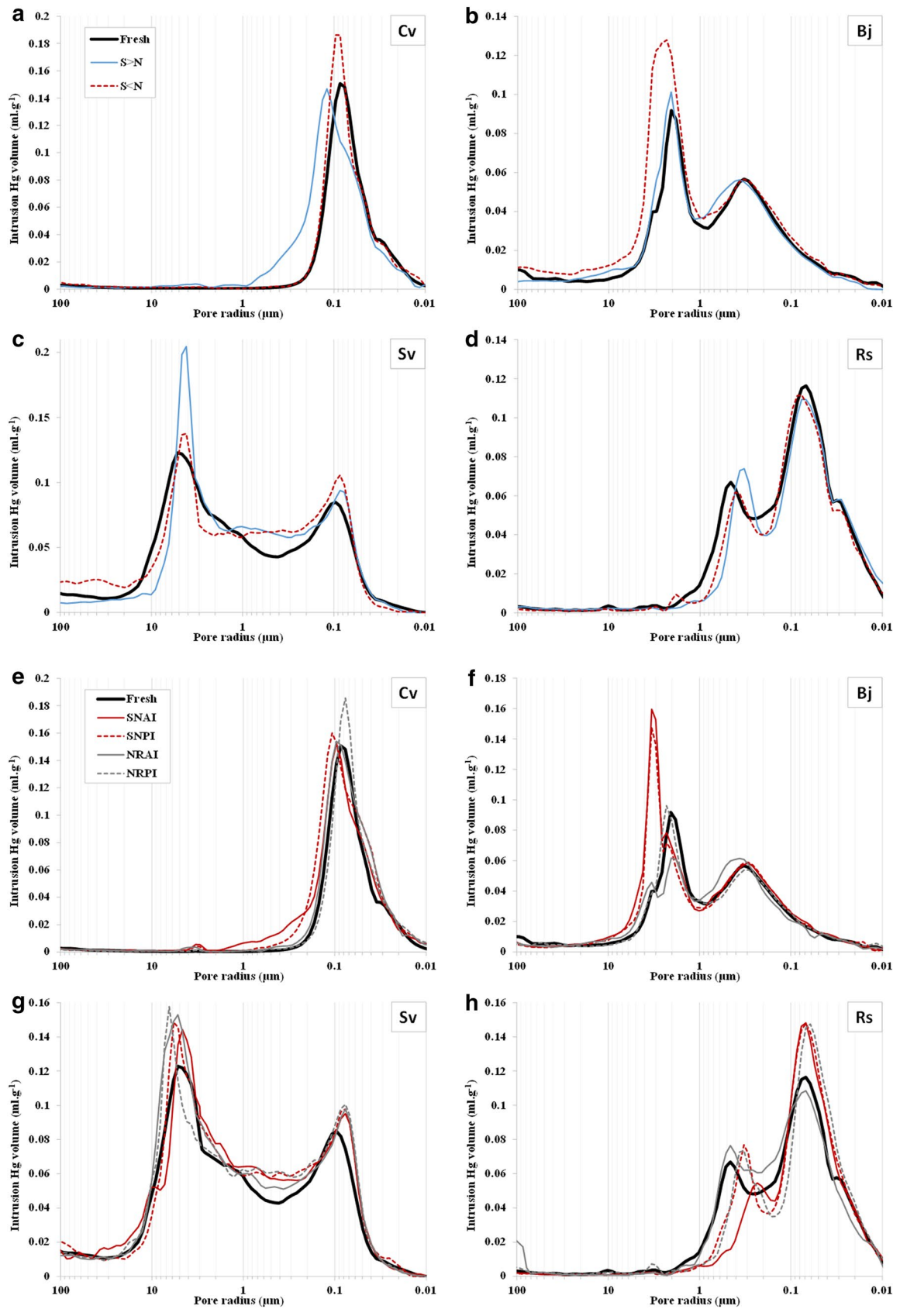


Fig. 7 Pore distribution before and at the end of the acid atmosphere exposures ($S > N$ symbolized the ratio $[H_2SO_3]/[HNO_3] = 4/1$ and $S < N$ symbolized $[H_2SO_3]/[HNO_3] = 1/3$) for Cv (a), Bj (b), Sv (c) and Rs (d). **b** Pore distribution before and at the end of the immersion tests (SNAI meant mixed acid in active immersion, NRAI for natural rain in active immersion, SNPI for mixed acid in passive immersion and NRAI for natural rain in passive immersion) for Cv (e), Bj (f), Sv (g) and Rs (h)

(2011) showed that laboratory experiments are difficult to extrapolate to on-site recession and generally overestimated due to the complexity of the rain composition.

This material loss was due to the calcite dissolution which was systematically two to four times higher in the acid solution and that depended on the porous system. Bigger pores lead to higher dissolution that explains the higher values in Bj and Sv. The calculus of the surface recession takes into account the dissolved components that explained the highest surface recession of the contaminated stones due to their sulfate-rich composition, especially in Rs in which the sulfate is combined with sodium, more soluble than gypsum (Thomachot-Schneider et al. 2016).

Differences active–passive

In the acid solution, the samples appeared more affected by the active immersion, while in the rainwater, the differences between active and passive effects were less distinctive. The weight loss and dissolved Ca^{2+} concentrations were two times higher in the active acid immersion. The active immersion catalyzed the reaction between acids and calcite considering the principle of the Collision Theory. This states that to achieve a reaction, molecules in solution must collide, thus the more collisions the faster the reaction is. The movement of the solution intensifies the motion rate of the reactant molecules increasing the chances of collision and consequently the production rate and the velocity of the reaction (Huber and Reid 1926; Shah et al. 2012). The agitation also generated mechanical effects which led to an erosion by the particles detachment (Baedeker and Reddy 1993; Camuffo 1995; Eyssautier-Chuine et al. 2016).

The rainwater solution was less acid with pH 5.9 than the acid solution with pH 5. The dissolution produced by this weak acidity needed more time to allow noticeable reactions for the sound stone and react preferentially on the previous gypsum in the contaminated stones. Indeed, even if the solution penetrated deeper in the porous network in active immersion (Eyssautier-Chuine et al. 2016), the chemical dissolution produced by the rainwater was comparable in active and in passive immersion. The only difference between both tests in the natural rainwater was the mechanical part of the erosion in active immersion that represented only a small fraction compared to the chemical dissolution of calcite as suggested by Bonazza et al. (2009).

Behavior of stones

Comparisons between fresh and initially contaminated stones

The presence of sulfates in the initially contaminated samples of Sv and Rs was confirmed by the ion chromatography results. Throughout the atmosphere tests, the quantity of the sulfur anions in Sv was constant, indicating that its initial calcium sulfate content limited the substitution reaction. The sodium sulfate present in Rs was dissolved due to the high RH of the test, and consequently calcium sulfate could precipitate. In both cases, the preexistent sulfate salts prevent the nitrate formation. Contrarily, the fresh stones, Cv and Bj, experimented an increase in sulfur and nitrogen concentration due to the substitution with Ca^{2+} . In addition, both fresh stones showed similar gypsum crystallization shape on their surface.

During the immersion tests, the loss of material was highlighted by the weight and the calcium content in stones decreasing more than twice for Sv and Rs. The presence of gypsum before the first immersion cycle in these two stones explained their higher dissolution due to the elevated solubility of sulfate salts compared to calcite (Camuffo 1995; Charola et al. 2007).

Influence of petrography

For all the tested stones, the first observation was the color change evidenced with naked eye and due to S deposition and metal elements oxidation. The samples showed a darkening after the mixed acid exposure, while the hue decreased similarly for both atmosphere exposition and acid immersion. Iron and manganese were detected in studied stones, with highest amount in Bj and Rs. The oxidized forms of Fe- and Mn-based compounds are darker than their reduced forms that explain the decrease in lightness (Völz et al. 2000). In addition, the Fe oxidation entailed a decrease in the hue of Cv and Sv, confirmed by the reddening of their surfaces. The transparent crust of gypsum crystals covering the surface of the atmosphere exposed samples could create interferences in light reflection that modified slightly the chromatic parameters (Vazquez et al. 2016).

In general, the total porosity varied slightly in mixed atmospheres and led to the widening of the pore access radii. The anionic substitution reaction led to a dissolution stage of the calcite preceding the salt crystallization. Both processes entailed variations, i.e., widening and closing, of the pore size distribution. The dissolution/crystallization process was noticed for all the stones within the two tests, independently of the S/N ratio. In Cv, the distribution was unimodal and the modifications affected the same pore size range, i.e., 0.1 μm of access radii, whereas the

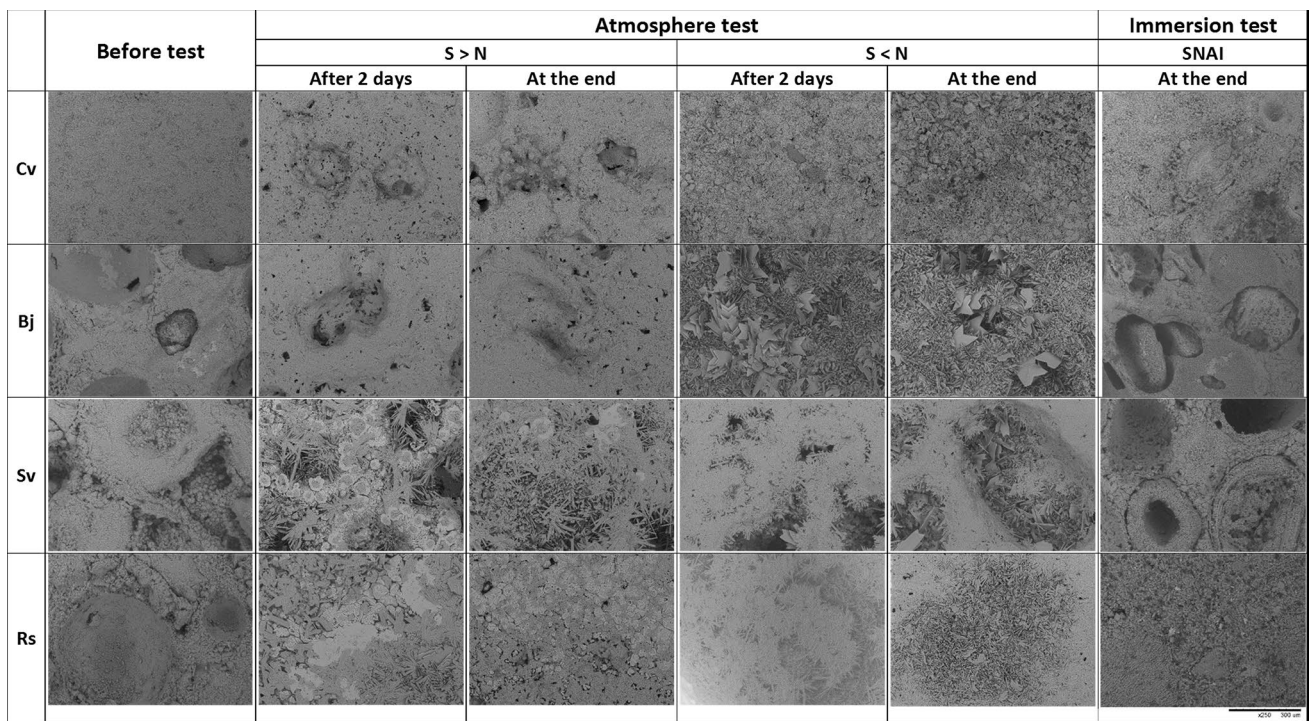


Fig. 8 SEM images of stone samples during the acid atmosphere and immersion tests

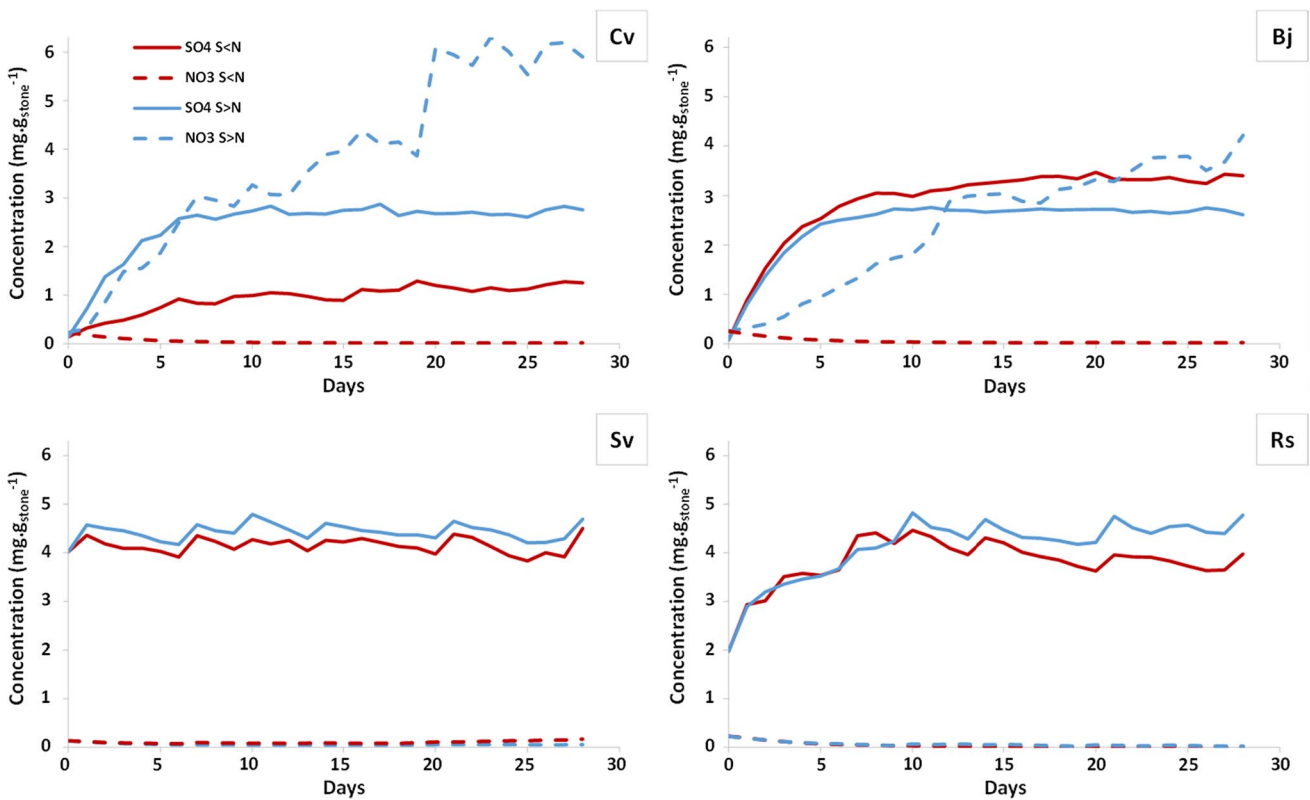


Fig. 9 Sulfates [SO_4^{2-}] (plain lines) and nitrates [NO_3^-] (dotted lines) content in stones during the S>N (blue lines) and S<N (red lines) exposures for each type of stone

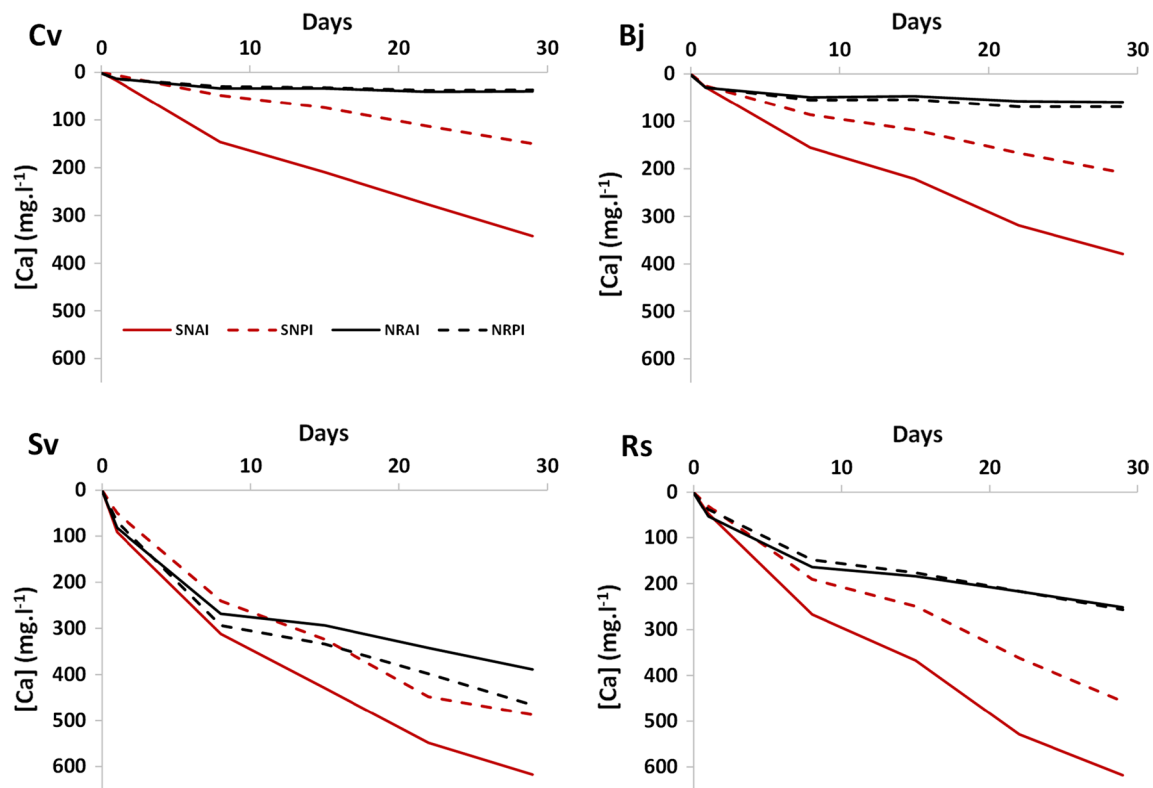


Fig. 10 Ca²⁺ concentrations in the immersion test solutions over time

Table 5 Calculated surface recession in function of the solution in immersion test, karst and acidity fractions and calibrated open porosity in function of calcite content [open porosity (%) multiplied by calcite content (%) from Eyssautier-Chuine et al. 2016]

	Natural rainwater (µm)	Acid solution (µm)	Karst effect (%)	Acidity effect (%)	Calibrated open porosity (%)
Cv	2	8	25	75	18.1
Bj	6	33	18	82	18.9
Sv	35	56	63	37	28.9
Rs	50	81	62	38	20.0

bimodality of the pore size distribution induced a variation in the entire pore network distribution, with aperture or closing depending on the different pore access sizes for each stone type.

During the immersion tests, Sv was the most affected regarding the weight and Ca losses that were explained not only by a faster and greater dissolution in high porous stones (Sabbioni and Zappia 1992; Bonazza et al. 2009) but also by the initial gypsum presence. That explains the lower dissolution in Bj which showed also large pore radii access and confirms that this parameter does not dominate the dissolution process.

Conclusions

In this study, the behavior of four stones exposed to past and future pollutants ratio, and the effect of acid rain storms was assessed and compared. The stone weathering caused by the effects of gaseous deposition and acid rain was evaluated by the submission of calcareous samples of three natural stones and an artificial one to accelerated aging tests. In the first test, the stone specimens were exposed to gaseous phase of two mixed acid solutions with different S/N ratios, and in the second one, the slabs were immersed in one artificial acid solution and in natural rainwater, in still and agitated conditions to simulate water stagnation and storms.

The SO₄²⁻/NO_x ratio plays a determining role in the alterations induced by the gaseous deposition. Higher the SO₄²⁻ amount is, more aggressive the weathering will be. The current pollution ratio (1:3) produces less intense color variations, mainly by the darkening of the stone surfaces due to compounds oxidation, and similar or lesser salt precipitation than in the past. After simulated rain tests, no salt crystallization was observed even if sulfates and nitrates were detected by ion chromatography. The material loss was mainly caused by the dissolution of calcite for all the stones and of the previous sulfates in the contaminated ones. The artificial acid solution was much more aggressive than the natural rainwater, suggesting that the acidity effect is

greater than the karst effect. In the mixed acid atmospheres, the change of the porous network depended further on the pore size distribution. In the immersion tests, the dominant parameter was the open porosity.

The differences between active and passive immersion were evident only for the acid solution, in which the samples appeared more affected by the active one. In rainwater immersion, the chemical dissolution was low due to the higher pH. In addition, the mechanical effect of the agitation represents a small part in the erosion process, and in this study it was insufficient to create differences between passive and active immersion. Thus, if natural rain acidity remains stable, the meteorological episodes such as strong storms will not induce a much higher stone deterioration.

In contaminated stones, the initial presence of sulfur compounds limited the crystallization of sulfates and nitrates in the acid atmosphere tests that make them unconcerned by the new and future atmospheric pollution ratio. In addition, these already existent salts will be leached sooner, protecting more the stone from dissolution decay than the fresh quarried ones.

Acknowledgements The authors want to thank Xavier Drothiere, Alexandra Conreux and Julien Hubert for their technical and analytical support.

Funding This study was funded by “Reims Métropole” with the project IFEPAR and the University of Reims-Champagne Ardenne and the “Ville de Reims” with the Project REMITHERM, and “Grand Est” with the project FLUTE.

Compliance with ethical standards

Conflict of interest The authors confirm that there is no conflict of interest in this research.

Informed consent Informed consent was obtained from all individual participants included in the study.

References

- Ansted DT (1860) On the decay and preservation of building materials. *J Franklin Inst* 70:155–163. [https://doi.org/10.1016/0016-0032\(60\)90149-6](https://doi.org/10.1016/0016-0032(60)90149-6)
- Baedecker PA, Reddy MM (1993) The erosion of carbonate stone by acid rain: laboratory and field investigations. *J Chem Educ* 70:104–108
- Bai Y, Thompson GE, Martinez-Ramirez S, Brüeggerhoff S (2003) Mineralogical study of salt crusts formed on historic building stones. *Sci Total Environ* 302:247–251
- Bai Y, Thompson GE, Martinez-Ramirez S (2006) Effects of NO₂ on oxidation mechanisms of atmospheric pollutant SO₂ over Baumberger sandstone. *Build Environ* 41:486–491. <https://doi.org/10.1016/j.buildenv.2005.02.007>
- Bionda D (2005) RUNSALT—a graphical user interface to the ECOS thermodynamic model for the prediction of the behaviour of salt mixtures under changing climate conditions. <http://science.sdf.eu.org/runsalt/>
- Bonazza A, Messina P, Sabbioni C et al (2009) Mapping the impact of climate change on surface recession of carbonate buildings in Europe. *Sci Total Environ* 407:2039–2050. <https://doi.org/10.1016/j.scitotenv.2008.10.067>
- Camaiti M, Bugani S, Bernardi E et al (2007) Effects of atmospheric NO_x on biocalcarene coated with different conservation products. *Appl Geochem* 22:1248–1254. <https://doi.org/10.1016/j.apgeochem.2007.03.035>
- Camuffo D (1995) Physical weathering of stones. *Sci Total Environ* 167:1–14
- Cardell-Fernández C, Vleugels G, Torfs K, Van Grieken R (2002) The processes dominating Ca dissolution of limestone when exposed to ambient atmospheric conditions as determined by comparing dissolution models. *Environ Geol* 43:160–171. <https://doi.org/10.1007/s00254-002-0640-x>
- CEN (Comité Européen de Normalisation) (2002) EN 13919: natural stone test methods: determination of resistance to ageing by SO₂ action in the presence of humidity. Brussels
- Charola AE, Pühringer J, Steiger M (2007) Gypsum: a review of its role in the deterioration of building materials. *Environ Geol* 52:339–352. <https://doi.org/10.1007/s00254-006-0566-9>
- CITEPA (2015) Inventaire des émissions de polluants atmosphériques et de gaz à effet de serre en France, Ministère de l'Écologie, du Développement durable et de l'Énergie. <http://www.citepa.org/fr/activites/inventaires-des-emissions/secten>
- Dewanckele J (2013) Spatial reorganization processes at a (sub)micron scale due to natural and artificial alteration inside natural stones. Ghent University, Ghent
- Dewanckele J, De Kock T, Fronteau G et al (2014) Neutron radiography and X-ray computed tomography for quantifying weathering and water uptake processes inside porous limestone used as building material. *Mater Charact* 88:86–99. <https://doi.org/10.1016/j.matchar.2013.12.007>
- Dolske DA (1995) Deposition of atmospheric pollutants to monuments, statues, and buildings. *Sci Total Environ* 167:15–31
- Eyssautier-Chuine S, Marin B, Thomachot-Schneider C et al (2016) Simulation of acid rain weathering effect on natural and artificial carbonate stones. *Environ Earth Sci* 75:1–19. <https://doi.org/10.1007/s12665-016-5555-z>
- Franzoni E, Sassoni E (2011) Correlation between microstructural characteristics and weight loss of natural stones exposed to simulated acid rain. *Sci Total Environ* 412:278–285. <https://doi.org/10.1016/j.scitotenv.2011.09.080>
- Fronteau G (2000) Comportements tégogénétiques des principaux calcaires de champagne-ardenne, en relation avec leur faciès de dépôt et leur séquençage diagénétique. Université d'Orléans
- Fronteau G, Moreau C, Thomachot-Schneider C, Barbin V (2010) Variability of some Lutetian building stones from the Paris Basin, from characterisation to conservation. *Eng Geol* 115:158–166. <https://doi.org/10.1016/j.enggeo.2009.08.001>
- Gardner ES (2006) Exponential smoothing: the state of the art—Part II. *Int J Forecast* 22:637–666. <https://doi.org/10.1016/j.ijforecast.2006.03.005>
- Graue B, Siegesmund S, Oyhantcabal P et al (2013) The effect of air pollution on stone decay: the decay of the Drachenfels trachyte in industrial, urban, and rural environments—a case study of the Cologne, Altenberg and Xanten cathedrals. *Environ Earth Sci* 69:1095–1124. <https://doi.org/10.1007/s12665-012-2161-6>
- Grossi CM, Murray M, Butlin RN (1995) Response of porous building stones to acid deposition. *Water Air Soil Pollut* 85:2713–2718. <https://doi.org/10.1007/BF01186244>
- Grossi CM, Brimblecombe P, Esbert RM, Alonso FJ (2007) Color changes in architectural limestones from pollution and cleaning. *Color Res Appl* 32:320–331. <https://doi.org/10.1002/col.20322>

- Haneef SJ, Johnson JB, Dickinson C et al (1992) Effect of dry deposition of NO_x and SO₂ gaseous pollutants on the degradation of calcareous building stones. *Atmos Environ* 26A:2963–2974
- Haneef SJ, Johnson JB, Thompson GE, Wood GC (1993) The degradation of coupled stones by wet deposition processes. *Corros Sci* 34:497–510. [https://doi.org/10.1016/0010-938X\(93\)90119-2](https://doi.org/10.1016/0010-938X(93)90119-2)
- Huber FC, Reid EE (1926) Influence of rate of stirring on reaction velocity. *Ind Eng Chem* 18:535–538. <https://doi.org/10.1021/ie50197a027>
- Kuhlman F (1863) New researches upon the preservation of building materials. *J Franklin Inst* 76:383–389. [https://doi.org/10.1016/0016-0032\(63\)90601-X](https://doi.org/10.1016/0016-0032(63)90601-X)
- Laycock EA, Spence K, Jefferson DP et al (2008) Testing the durability of limestone for cathedral façade restoration. *Environ Geol* 56:521–528. <https://doi.org/10.1007/s00254-008-1333-x>
- Lipfert F (1989) Atmospheric damage to calcareous stones: comparison and reconciliation of recent experimental findings. *Atmos Environ* (1967) 23:415–429
- Livingston RA (1992) Graphic methods for examining the effect of sulphur dioxide on carbonate stones. In: Proceedings of 7th international congress deterioration and conservation of stone, Laboratorio Nacional de Engenharia Civil, Lisbon, pp 375–386
- Massey SW (1999) The effects of ozone and NO_x on the deterioration of calcareous stone. *Sci Total Environ* 227:109–121
- Monna F, Puertas A, Lévêque F et al (2008) Geochemical records of limestone façades exposed to urban atmospheric contamination as monitoring tools? *Atmos Environ* 42:999–1011. <https://doi.org/10.1016/j.atmosenv.2007.10.021>
- Price CA (2000) An expert chemical model for determining the environmental conditions needed to prevent salt damage in porous materials. European Commission Research Report No 11, (Protection and Conservation of European Cultural Heritage) Archetype Publications, London
- Reddy MM (1988) Acid rain damage to carbonate stone: a quantitative assessment based on the aqueous geochemistry of rainfall runoff from stone. *Earth Surf Process Landforms* 13:335–354. <https://doi.org/10.1002/esp.3290130406>
- Reeder RJ (ed) (1983) Carbonates: mineralogy and chemistry. *Rev Mineral Mineralog Soc Am* 11
- Rodriguez-Navarro C, Sebastian E (1996) Role of particulate matter from vehicle exhaust on porous building stones (limestone) sulfation. *Sci Total Environ* 187:79–91
- Ross M, McGee ES, Ross DR (1989) Chemical and mineralogical effects of acid deposition on Shelburne Marble and Salem Limestone test samples placed at four NAPAP weather-monitoring sites. *Am Miner* 74:367
- Sabbioni C, Zappia G (1992) Decay of sandstone in urban areas correlated with atmospheric aerosol. *Water Air Soil Pollut* 63:305–316. <https://doi.org/10.1007/BF00475497>
- Shah SIA, Kostiuk LW, Kresta SM (2012) The effects of mixing, reaction rates, and stoichiometry on yield for mixing sensitive reactions 2014; Part I: model development. *Int J Chem Eng* 2012:16
- Simao J, Ruiz-Agudo E, Rodriguez-Navarro C (2006) Effects of particulate matter from gasoline and diesel vehicle exhaust emissions on silicate stones sulfation. *Atmos Environ* 40:6905–6917. <https://doi.org/10.1016/j.atmosenv.2006.06.016>
- Tecer L (1999) Laboratory experiments on the investigation of the effects of sulphuric acid on the deterioration of carbonate stones and surface corrosion. *Water Air Soil Pollut* 114:1–12. <https://doi.org/10.1023/A:1005177201808>
- Thomachot-Schneider C, Gommeaux M, Fronteau G et al (2011) A comparison of the properties and salt weathering susceptibility of natural and reconstituted stones of the Orval Abbey (Belgium). *Environ Earth Sci* 63:1447–1461. <https://doi.org/10.1007/s12665-010-0743-8>
- Thomachot-Schneider C, Gommeaux M, Lelarge N et al (2016) Relationship between Na₂SO₄ concentration and thermal response of reconstituted stone in the laboratory and on site. *Environ Earth Sci*. <https://doi.org/10.1007/s12665-016-5388-9>
- Török Á, Rozgonyi N (2004) Morphology and mineralogy of weathering crusts on highly porous oolitic limestones, a case study from Budapest. *Environ Geol*. <https://doi.org/10.1007/s00254-004-1036-x>
- Török Á, Licha T, Simon K, Siegesmund S (2011) Urban and rural limestone weathering: the contribution of dust to black crust formation. *Environ Earth Sci* 63:675–693. <https://doi.org/10.1007/s12665-010-0737-6>
- Vazquez P, Alonso FJ (2015) Colour and roughness measurements as NDT to evaluate ornamental granite decay. *Proc Earth Planet Sci* 15:213–218
- Vazquez P, Luque A, Alonso FJ, Grossi CM (2013) Surface changes on crystalline stones due to salt crystallisation. *Environ Earth Sci* 69:1237–1248. <https://doi.org/10.1007/s12665-012-2003-6>
- Vazquez P, Carrizo L, Thomachot-Schneider C et al (2016) Influence of surface finish and composition on the deterioration of building stones exposed to acid atmospheres. *Constr Build Mater* 106:392–403. <https://doi.org/10.1016/j.conbuildmat.2015.12.125>
- Völz HG, Kischkewitz J, Woditsch P et al (2000) Pigments, inorganic. In: Ullmann's encyclopedia of industrial chemistry. Wiley-VCH Verlag GmbH & Co., KGaA
- Webb AH, Bawden RJ, Busby AK, Hopkins JN (1992) Studies on the effects of air pollution on limestone degradation in Great Britain. *Atmos Environ Part B Urban Atmos* 26:165–181